3D PRINTING AND ADDITIVE MANUFACTURING
Volume 00, Number 00, 2019

DOI: 10.1089/3dp.2018.0117

Zero-Support 3D Printing of Thermoset Silicone Via Simultaneous Control of Both Reaction Kinetics and Transient Rheology

Stephanie Walker,[1,2] Uranbileg Daalkhaijav,[3] Dylan Thrush,[4] Callie Branyan,[2] Osman Dogan Yirmibesoglu,[2] Gina Olson,[2,4] and Yigit Menguc[2,*]

Abstract

This article presents a framework for using isothermal curing kinetics and transient rheological data to 3D print a curing thermoset silicone without support. These data are used to determine time and temperature boundary conditions for amount of curing during extrusion and layering of the print. From the time of mixing, rheological data show how the elastic modulus (G') and yield stress (σ_y) grow as the number of crosslinks increases. The kinetics data show changes in the rate of curing of the silicone and predict final cure time. Time boundaries for stages of transient curing are reported from heat flow, yield stress, and G' at the printer operating temperature. These times are used to prevent clogging of the mixing nozzle and ensure layering of unsupported elastomeric silicone. Several models are 3D printed to show the successes and drawbacks of the method within equipment limitations. This framework can be applied to help bound the printable region of other reactive thermoset materials in mixed extrusion systems. By printing without support, this method can produce overhanging and enclosed hollow structures that require minimal postprocessing.

Keywords: 3D printing, soft robotics, kinetics, rheology, silicone

Introduction

Direct extrusion 3D printing of silicones enables the creation of customizable soft devices. Several previous solutions in direct extrusion 3D printing of silicone have been developed for research purposes[1–12] and commercial products/services.[13–18] Silicone elastomers provide the benefit of potentially highly stretchable behavior depending on formulation. 3D printing those silicones as a fabrication method enables customizability, and with a wide range of material properties to choose from, specifically for two-part room temperature vulcanizing (RTV-2) silicones, optimizing 3D printing systems to take advantage of these properties is needed.

Ultimately, the properties that make silicone thermosets desirable for soft devices (high elasticity, low stiffness, and simple two-part chemistry) also make direct extrusion 3D printing with these silicones difficult. Their inherent softness in the uncured state can make the layers deform during printing. One solution for the softness or low viscosity is to print these silicones with sacrificial support material or in a support bath.[15,19–21] But development of printing strategies without the use of a bath is important in situations where drainage of the bath material may be difficult or impossible. Their two-part chemistry also means that they must be mixed before extrusion. 3D printers have been designed to mix multiple materials together while extruding,[5,7,8,22] and the research papers most relevant to this work have developed mixing extruder heads capable of 3D printing reactive materials. In this work, we build on this initial idea of 3D printing reactive silicone and dive deeper into the material-level control of the cure to enhance silicone print quality without support material.

[1]Department of Materials Science, Oregon State University, Corvallis, Oregon.
[2]Collaborative Robotics and Intelligent Systems (CoRIS) Institute, Oregon State University, Corvallis, Oregon.
[3]Department of Chemical, Biological, and Environmental Engineering, Oregon State University, Corvallis, Oregon.
[4]Department of Mechanical Engineering, Oregon State University, Corvallis, Oregon.
Current affiliation: Facebook Reality Labs, Redmond, Washington.

Opposite page: Here a small 3D printed silicone octopus has been cut open to reveal a hollow interior. Controlling transient rheology and curing kinetics during silicone 3D printing allows for the creation of these interior voids and overhanging geometries without support material. *Photo Credit:* Callie Branyan.

For 3D printing of structured fluids such as silicone elastomers, emphasis is placed on tailoring their rheological properties to achieve the desired processability and print fidelity.[23] Yield stress (σ_y), elastic modulus (G'), and shear thinning characteristics are commonly characterized as key parameters describing viscoelastic fluid behavior. To our knowledge, no curing kinetics characterization exists for the transient material properties of the popular Dragon Skin silicone system from Smooth-On, especially for a 3D printer with a mixing extruder. Previous research has also not revealed methods for controlling the transient curing properties of these RTV-2 silicones to make better 3D prints. Characterizing the amount of cure versus rheological properties (like G' and σ_y) makes it possible to ensure fluid-like behavior as the material is extruded and solid-like behavior after extrusion. Ensuring solid-like behavior after extrusion enables 3D printing of complex models with overhangs and hollow features without the use of support.

However, the characterization of transient curing and structural properties for reactive materials in mixed extrusion systems has been limited. Using a heated build chamber for increasing stiffness in a fluid print is noted as a solution to prevent collapse of the structure.[24] However, characterizing transient rheological properties that occur when 3D printing a curing material has not been the focus of previous work. A common strategy is to increase the cure time of the silicone through cure retarding additives or to extrude quickly before material properties significantly change.[9,12] But by controlling the RTV-2 transient curing behavior, longer print times and more stiffness can be achieved. As the RTV-2 silicone cures, its σ_y and G' will vary with time and (potentially) temperature due to the development of crosslinks in the polymer. Characterizing this transience enables better control of material behavior in the curing silicone and creates opportunities for better print quality.

In this work, we present a framework for determining the optimal time and temperature boundaries for 3D printing mixed thermoset silicone. This framework is built upon the translation of rheological and curing kinetics data into time and temperature boundary conditions for a silicone printer with in-line mixing. Prints are possible at a high resolution comparable with current thermoplastic printing technology ($\sim 500\,\mu$m). We utilize rheological characterization to determine the transient growth of the thermoset polymer's σ_y and G', then compare this behavior with isothermal curing kinetics to bound the time and temperature ranges for the best amount of crosslinking for layering. Printed sample geometries demonstrate the applicability of the framework for soft components and actuators with overhangs, high aspect ratios, and hollow cavities.

Materials and Methods

Formulation

To enable extrusion and layering, a new silicone formulation was created. This formulation was (by weight) as follows: 87.3% Dragon Skin™ 10 Very Fast Part A (or B), 0.98% Thi-Vex, 9.8% Silicone Thinner, and 1.96% Silc-Pig Dye (all from Smooth-On). Supplementary Figure S1 (Supplemental Data) explains the formulation development. For printing and testing, mixture A (Part A + Thi-Vex + Silicone Thinner + Dye) and mixture B (Part B + Thi-Vex + Silicone Thinner + Dye) were each preloaded into a syringe.

Rheological characterization

Rheological characterization was performed to determine the relationship of the elastic modulus G' and loss modulus G'' to time (curing tests), and to monitor yield stress as curing progressed. All rheological tests were performed on an AR2000ex rotational rheometer with 40 mm parallel plate geometry (TA Instruments). To prepare each sample, Syringe A and Syringe B were mixed 1:1 by weight in a Thinky AR-310 Planetary Centrifugal Mixer for 15 s at 2000 rpm and then for 15 s at 2200 rpm. After mixing, each sample was spread in-between the preheated parallel plate geometry by the time that ~ 2 min from mixing had elapsed. Once the sample was loaded, excess silicone was wiped away and the test began immediately (or at increasing time intervals in the case of yield stress tests). A new sample was used for each test.

Cure tests were performed as isothermal oscillatory shear tests at 0.5% strain and 10 rad/s angular frequency in triplicate for a range of temperatures (25°C, 30°C, 35°C, and 40°C). Each test recorded the behavior of G' and G'' over time until the G' data reached a plateau, signifying near full cure. The resulting data were used to eliminate operating temperatures that would cause the silicone to cure too quickly for smooth extrusion. Comparing G' near the end of the curing process to the curing kinetics data also helped confirm the time of full cure.

Yield stress tests were performed to determine at what time the last rheologically measurable yield stress occurred in the silicone at 30°C and 35°C. After sample loading, the silicone was sheared at a constant $0.02\,s^{-1}$ shear rate for 3 min, while the resulting stress values were recorded (stress growth test). During this time, the first local stress maximum after the test began (yield stress) occurred. Each sample was loaded into the rheometer at the same time after mixing, but shearing was started at increments of 1 min up until the torque limit on the rheometer was reached. For example, a ''5 minute start time'' sample was loaded at 0 min, left on the machine for 5 min, and then the yield stress test began.

Curing kinetics characterization

Curing kinetics characterization was performed to help find the time of maximum rate of cure and the time of full cure. Isothermal experiments were performed on a differential scanning calorimeter (DSC Q2000 [TA Instruments]). During these tests, heat flow data versus time were collected. To connect these data to curing behavior, it was assumed that heat flow was proportional to the number of crosslinks formed. To prepare the sample, Syringe A and Syringe B were mixed 1:1 by weight in a Thinky AR-310 Planetary Centrifugal Mixer for 15 s at 2000 rpm and then 15 s at 2200 rpm. Each mixed sample was then loaded through syringe into an aluminum hermetic pan and sealed with a lid. Sample masses ranged from 10.4 to 13.1 g. The sealed sample was placed into the preheated furnace by the time that ~ 2 min from mixing had elapsed. The chamber environment was purged with a nitrogen atmosphere at 50 mL/min. Each sample was heated until the heat flow signal did not change for at least 3 min. The point at which the heat flow was unchanging signaled the end of cure assuming no residual reaction(s). Three samples were run at each temperature (25°C, 30°C, 35°C, and 40°C), and their resulting heat flow versus time data were averaged per temperature.

Printer setup

The printer consists of a commercial gantry inside of a heated chamber with a custom mixing extruder. The design specifics are explained more thoroughly in the Supplemental Data. In brief, to begin printing, Syringe A and Syringe B were placed in the syringe pump and attached to fluid lines that connected to the top of the mixer. The heater was then turned on to allow the inner chamber to reach the set temperature. Before pumping the silicone, the mixer and reamer were cleaned and reinstalled, and the mixer was turned on. Then the syringe pump was run at 1 mL/min for ~3 min to flush the system. A clean nozzle was then attached to the bottom of the mixer, and the flow rate on the pump was brought to 0.2 mL/min for 2–8 min followed by a 0.0385 mL/min equilibrium flow rate (set on the syringe pump). The silicone was initially tested in the extrusion system at operating temperatures starting at 30°C to determine the maximum operating temperature. Testing consisted of trying to extrude the silicone with the mixer running after the printer had reached the set temperature. The maximum operating temperature was determined when the flow of the silicone was smooth and consistent, without the filament extruding in irregular shapes.

Several supplementary tests were performed to enable printing of the silicone. These included normal force testing to estimate the weight the silicone could hold while curing (Supplemental Data, Section Normal Force Methods), filament spanning tests (Supplemental Data, Section Spanning Tests), and filament dimensional analysis through profilometry (Supplemental Data, Section Line Height Profilometry).

Demonstration prints

Demonstration prints were made to test the feasibility of fabricating hollow and overhanging geometries within the previously determined printing time window at 30°C. First, a 3D overhang test model with angles from 25° to 70° was printed to determine the possible maximum overhang angle without visible sagging of the silicone. Then, five more example prints of similar scale were made to explore various combinations of overhang angles. Example prints were all hollow and included an octopus, a licorice-shaped cylinder, a pyramid with a 30° overhang angle, an eggshell, and a bellows. To ensure that each model would print properly, their size was increased until a successful print was completed. If the print was too small, each layer would not be crosslinked enough to hold weight. A pneumatic actuator was also printed as an example for soft robotics. After printing the actuator, a few stray filaments were cut, and a pneumatic tube was glued into the model. The actuator was then inflated from 0 to 23.6 kPa. The resulting curvature of the actuator was determined by fitting a circle to the interior curve of the actuator and noting its radius.

Results

Figure 1 outlines the overall process for using rheology and curing kinetics data for the silicone printer development and operation. While formulation of the silicone was important to ensure initial extrudability and structural integrity while printing (Fig. 1a and Supplementary Fig. S1), the inclusion of rheology and curing kinetics data was integral for

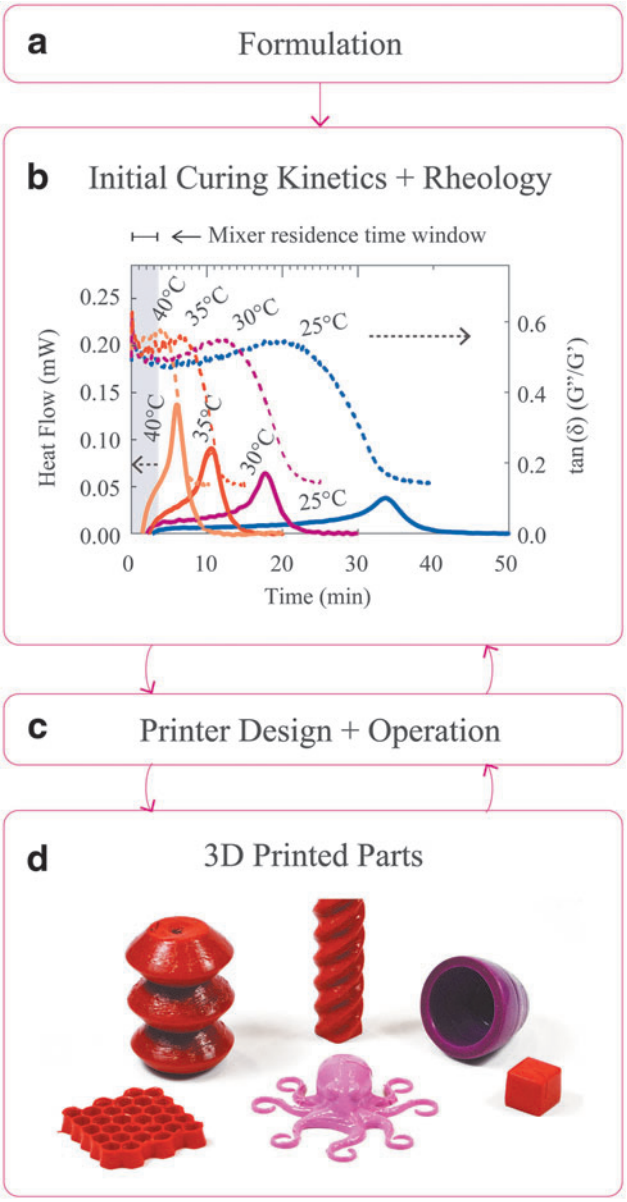

FIG. 1. It is advantageous to use rheological and curing kinetics data for custom isothermal printer development to determine the highest operating temperatures possible for the machine. Here a flowchart is presented on how rheology and curing kinetics were implemented during the printer development process. **(a)** First, a silicone formulation was created, which could be extruded through a high-resolution nozzle and also clearly had a yield stress that would keep filament structure after extrusion. **(b)** Second, isothermal curing kinetics and rheological testing were performed to get an idea of how the silicone material properties changed with time and temperature. Operating at the highest possible temperature when extruding a thermally curing material decreased print time by increasing the number of crosslinks (and therefore silicone stiffness) while layers were deposited. This increase in stiffness enabled the printing of complex geometries (hollow and overhanging without support). **(c)** Third, a printer design was created to accommodate the need for in-line mixing, isothermal heating, and pumping of high-viscosity polymers. **(d)** Finally, because of all this preparation and characterization, 3D prints with overhangs and hollow regions are possible at resolutions close to traditional FDM printers (~335–500 μm).

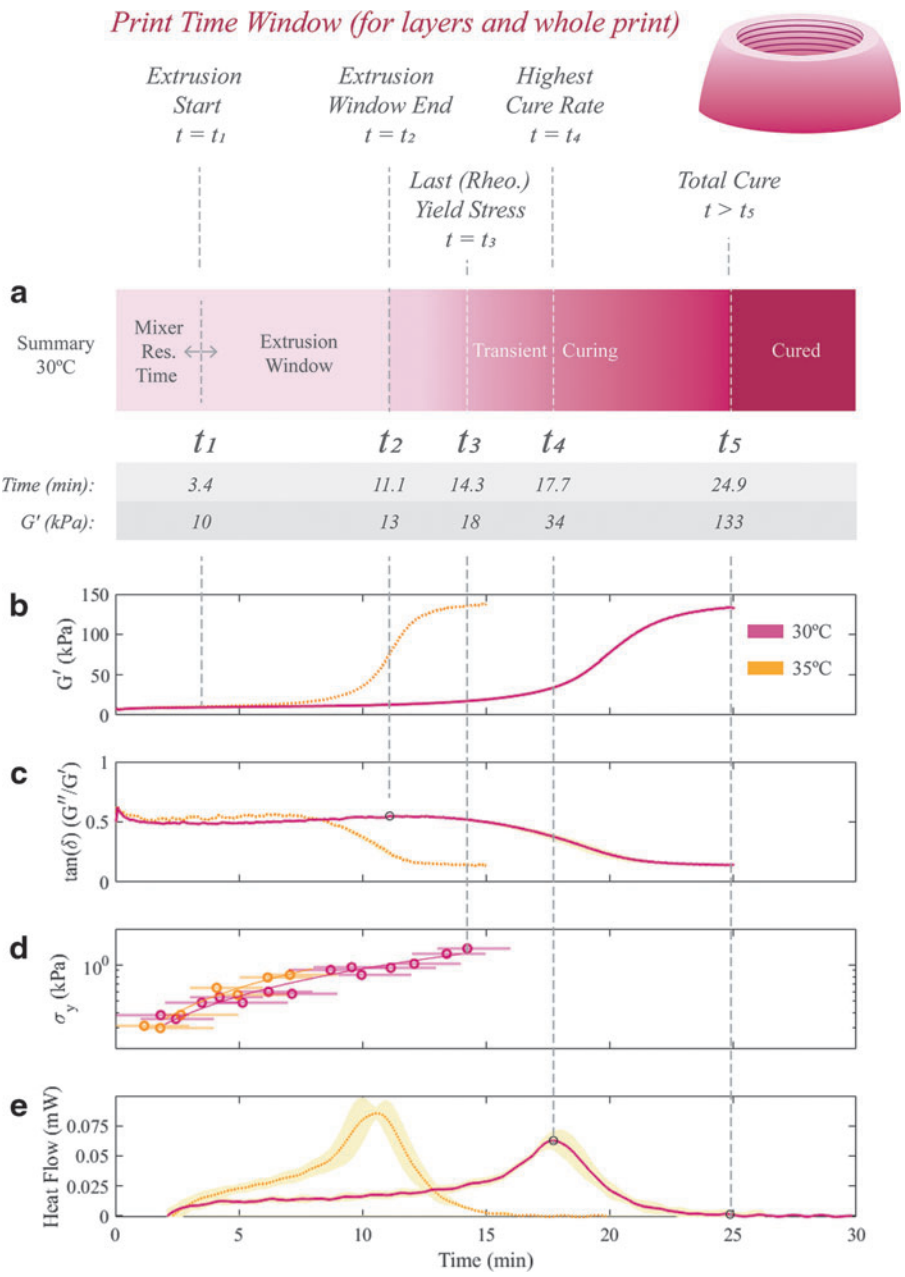

FIG. 2. **(a)** The amount of crosslinking in the silicone can be controlled by operating the printer within specific temperatures and times bound with rheological and curing kinetics data and equipment limitations. A summary curing gradient for 30°C shows the important points of note: the mixer residence time t_1, the maximum just before the decrease in tan(δ) t_2, the point of last yield stress measurable through rheometer t_3, the point of fastest cure rate t_4, and the final cure time t_5. **(b)** The growth of G' after mixing is useful to compare with all data sets because it increases with the amount of crosslinks developed in the material, which positively correlates to the silicone stiffness. **(c)** The rheological curing data show the behavior of tan(δ) from the just mixed state to the full cure state. The time period just before the decrease in tan(δ) (t_2) is a good time to extrude the polymer because G' does not significantly change from its initial mixed value during this time. After this point, G' starts to increase, and so extrusion will become more difficult because of crosslinking in the silicone. **(d)** The yield stress value of the curing silicone increases as it cures. The last yield stress presented is the last yield stress measurable through the rheometer. The horizontal bars represent the test time range for each yield stress data point. A yield stress is necessary to reduce disruptions possible from nozzle interactions and the weight of printed layers. **(e)** Heat flow is directly proportional to rate of cure, with the highest cure rate occurring at the peak in the data. At this point, the silicone retains its uncured state but the structure is stiffer. When the heat flow signal shows no change over time near the end of the data, the silicone is cured.

understanding transient material behavior and bounding the printer operating times and temperatures according to cure state (Fig. 1b). This preparation enabled the design and operation of a custom printer (Fig. 1c) for the printing of silicone with overhangs and hollow regions (Fig. 1d).

Rheology and curing kinetics data were initially used to omit too high or too low operating temperatures from the initial range of 25°C, 30°C, 35°C, and 40°C. For extrusion, the mixer residence time of 3.4 min needed to be lower than the time where the G' growth rate started to increase significantly due to an increase in crosslinking. The relationship between G' and G'' seen in tan(δ) (G''/G') showed that the growth of G' outpaced G'' right after tan(δ) reached a maximum, after which tan(δ) quickly decreased (Fig. 1b, right y axis). This sudden decrease in tan(δ) occurred at $\sim$4 min in the 40°C data, which was too close to the residence time of the mixer and would increase the chances of clogging. So, 40°C was omitted. The 25°C operating temperature was then omitted because the curing kinetics data showed that the time of full cure (the point when the data flatten out for several minutes) occurred at 40 min at this temperature. This was too long for realistic print times. The remaining temperatures (30°C and 35°C) were tested with the custom mixing extruder inside the heated printer. At 30°C, the silicone flowed smoothly out of the nozzle, and the material retained qualitatively sufficient structure. When printing above this temperature, the extrusion was irregular, with clogging occurring more quickly than at 30°C. So, 30°C was used for all printing experiments.

To further bound the printing time window at 30°C, tan(δ), G' growth, heat flow, and yield stress (σ_y) data were overlaid on the same time scale (Fig. 2). This scale outlined important regions of time to consider for extrusion, layering, and full cure of the silicone prints. The 35°C data were also overlaid as a reference, which gave insight into the structural growth of the curing silicone at a higher temperature, even though this temperature was not usable for our system. The print time window began after mixing and continued until the end of curing (Fig. 2a left to right). Points of importance are described in the following section.

In order of increasing time, the first notable point was t_1, the residence time of the mixer (3.4 min). The mixer residence time needed to be low enough to avoid significant growth of G' before extrusion (Fig. 2b). The second point t_2 (11.1 min) was the boundary for solid-like growth in the silicone (Fig. 2c). This point was the maximum value of tan(δ) (G''/G') occurring before tan(δ)'s rapid decrease. The rapid decrease in tan(δ) during curing showed the rapid growth of G' over G'', a signal for the increase in solid-like behavior through acceleration of cure. At t_2, the G' value (13 kPa) had also increased by <3% of the difference between its full cure (133 kPa) and just mixed value (10 kPa). The growth of G' and G'' at all temperatures is compared in Supplementary Figure S2.

The presence of a yield stress in the silicone was important to ensure that the uncured filament could be layered. Data at 30°C and 35°C showed that even in the just mixed state, the silicone had a yield stress (Fig. 2d). After mixing, the yield stress of the silicone steadily increased until the material became too cured to have a yield stress measurable within the instrument limitations. The point of last yield stress at 30°C was t_3 (14.3 min), and this value correlated to a G' value of 18 kPa. Each yield stress point before t_3 in the plot was the yield stress value of the silicone for a specific test start time.

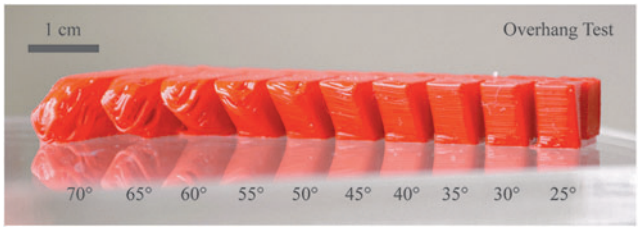

FIG. 3. The overhang test print shows that past a 35° overhang angle the print starts to sag slightly with a more obvious sagging at 45°. Beyond this, the silicone does not hold overhanging features at this print size. This was used to help determine the limit of printability for overhang geometries in this system.

The curing kinetics data revealed two more important points. The first was the time of highest rate of cure, t_4, which occurred at the peak heat flow value at 17.7 min (Fig. 2e) and correlated to a G' value of 34 kPa. At this point, the silicone had a stiffer yet still uncured state. The last point was the time of full cure, t_5 (24.9 min), which correlated to the highest G' value of 133 kPa (Fig. 2e). The heat flow cure time also matched well with the end of the G' plateau.

Printed models

3D printing of the silicone between t_1 and t_5 led to some important insights about printable overhang geometries. The overhang test print gave the geometrical limit of overhanging structures as $\sim$35° from the vertical before sagging occurred (Fig. 3). The other print demonstrations (octopus, licorice, pyramid, eggshell, and bellows) displayed a range of printable heights and overhanging geometries as well as some of the limitations of the printing method (Fig. 4). The prints are shown in order of increasing difficulty (Fig. 4a) and are qualitatively compared with their STL models (Fig. 4b). The pyramid has an $\sim$30° overhang, which shows no signs of sagging. The interior cross-sections of the eggshell and bellows (most difficult) models show that once the overhang angle threshold is passed the print quality is unpredictable (Fig. 4c). Close-up views also show good quality surface finish (Fig. 4d). Print time for each model (Fig. 4e) can be compared with the time chart in Figure 2. The 3D printed hollow pneumatic actuator (Fig. 5) curls under pressure with a radius of curvature that decreases in an approximately linear trend. Supplementary Movie S1 shows the printing process in more detail.

Discussion

3D printing silicone without support enables the fabrication of hollow soft morphologies that are difficult to create through molding and 2D lamination methods. To print RTV-2 silicones, transient material properties must be controlled because (1) mixing is required for the material to cure, which creates a time limit on printability and (2) increased temperatures are required to increase silicone stiffness within reasonable time frames. Cure retarding additives can reduce the curing speed of an RTV-2 silicone to reduce chances of clogging, but this choice relies on layering the silicone in a

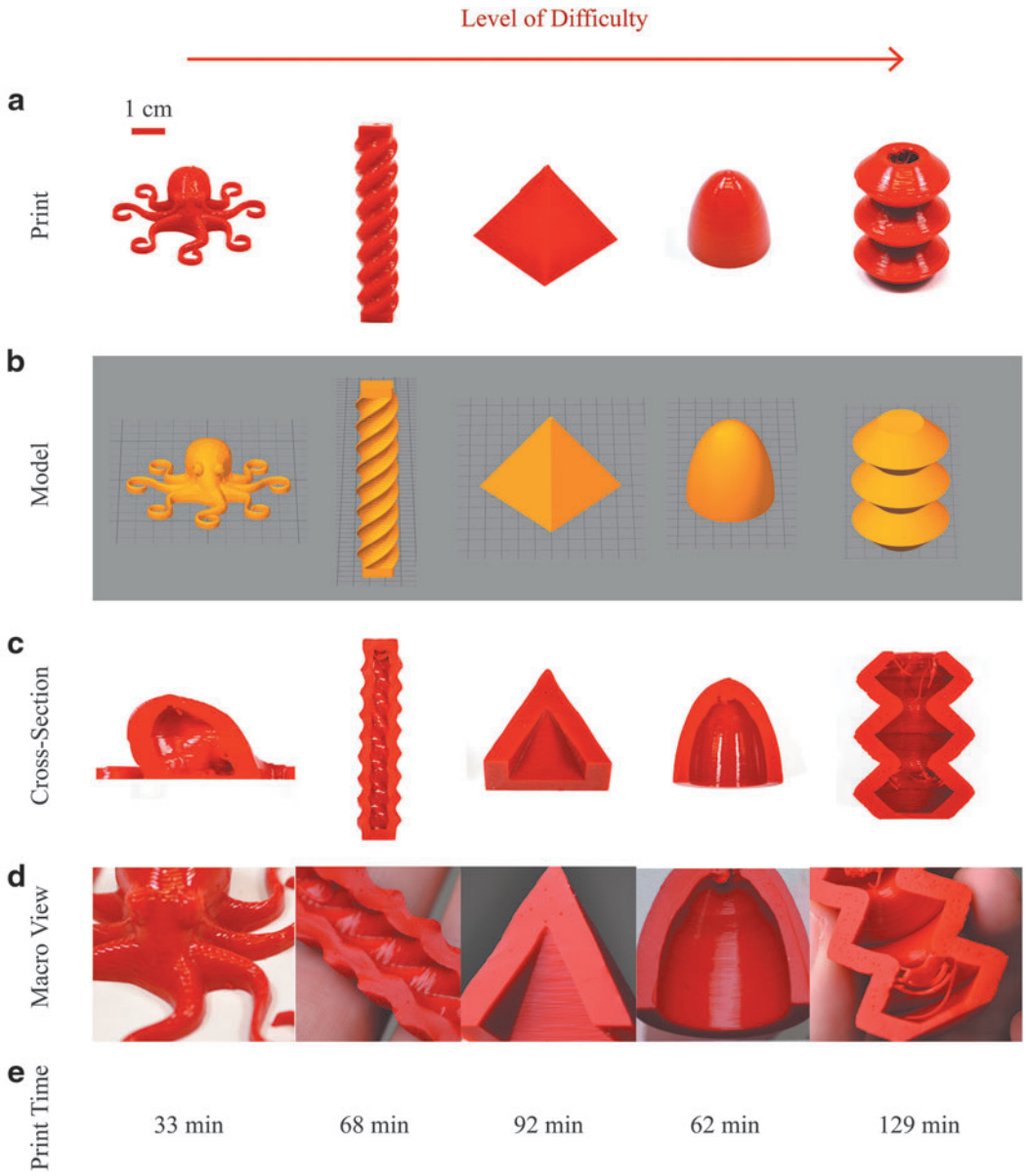

FIG. 4. **(a)** Tall, hollow, and overhang prints are possible when working within the time and temperature boundaries specified by rheology and curing kinetics. **(b)** The 3D CAD models are sliced according to line profilometry estimates for the dimensions of the cured filaments. **(c)** Cross-sections of prints show that overhang and hollow geometries work well up to $\sim 35°$ angle from the vertical as predicted from the overhang test. For example, the pyramid has an $\sim 30°$ overhang, which holds up until the structure is finished printing. Once the angle threshold is passed, or if the material does not have enough stiffness, sagging occurs in the unsupported filaments and the structure collapses. This is especially evident in the bellows structure with its 45° angle overhangs and high spanning lengths on the top of the model. Although the 45° angle is possible to print with some sagging, the results are unpredictable. The licorice and eggshell-shaped prints show the same behavior where there is a high overhang angle or where spanning over unsupported regions is needed. **(d)** Macroviews show close-ups of the print quality. The resolution on this printing system (~ 335–$500\ \mu$m) is comparable with traditional FDM printers. **(e)** The print time for each model is shown to compare with the time chart from the rheological and curing kinetics in Figure 2. As each model is printed, there are areas that are uncured, have transient curing, or are fully cured. It should be noted that prints like the octopus, which are small and short, are possible to print with a relatively short time period per layer because the silicone has an initial yield stress and can hold some weight even in the just mixed state. As the models become heavier and more complex, more support from the crosslinking occurring in previously deposited layers is needed to ensure that the printed structure does not collapse due to the weight of the newly deposited silicone.

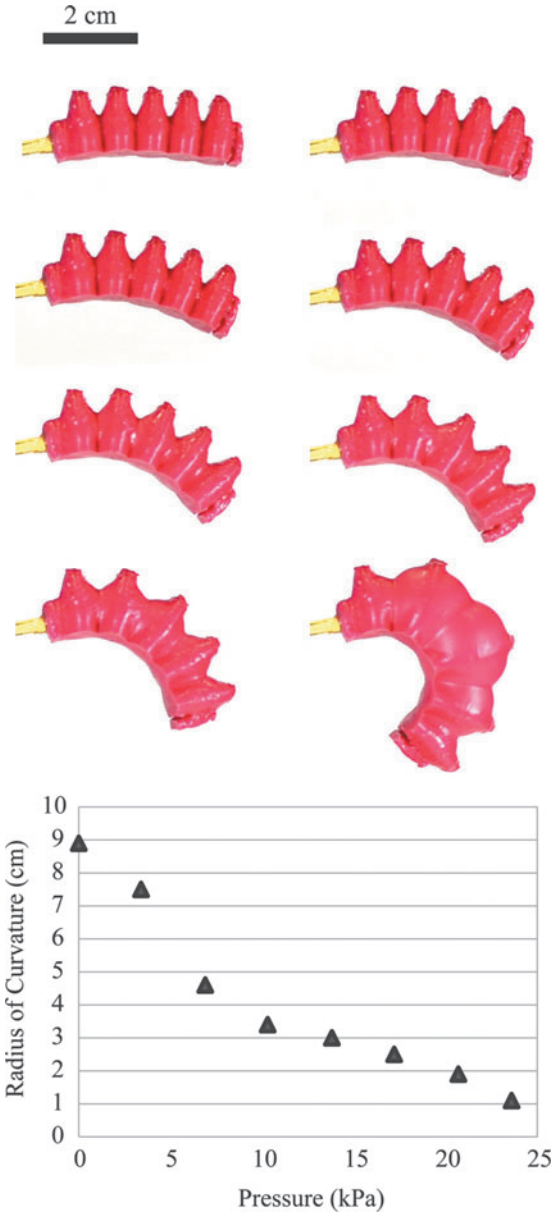

FIG. 5. Hollow actuators can be 3D printed without the use of support. Here a brief characterization of pressure versus radius of curvature (R) in a bellows-*shaped* actuator is shown.

fully uncured state, which limits the morphologies to those without large hollow regions or those that require a support material. To create stiffer silicone during printing, a heating system can be implemented.[8] But controlling the application of heat over time is even more important to prevent clogging and ensure stiff layers. Transient rheological and curing kinetics data under isothermal conditions bound optimal print temperature(s) and time(s), and can be coordinated with specific equipment limitations. The important points from the rheological and curing kinetics characterization represent easily identifiable material changes obtainable through common methods. While the exact times of the important points may be different for each material, the overall concept is the same. Each of the important times in the curing window has different impacts on the printing process and is discussed in the following paragraphs.

The relationship between t_1 and t_2 helps ensure proper extrusion. The residence time of the mixer needs to enable extrusion before t_2 without a fundamental change in G' behavior. Designing smaller mixers or using higher flow rates would reduce this residence time, and therefore allow for an increase in operating temperature. As seen in the data in Figure 1, silicone printing at higher temperatures such as 40°C could be possible if the mixer residence time was reduced. The time when G' increases/tan(δ) decreases is a good general boundary for extrusion due to the expectation that the amount of crosslinking (and therefore stiffness) can be related to G' growth. Using this logic, extrusion should have also been possible at 35°C. However, when running the extruder at anything >30°C, the filament shape was irregular and the nozzle would clog. Future work is planned to further investigate what could be causing this discrepancy.

It is useful to know points t_3, t_4, and t_5 for silicone layering. The last measurable yield stress on the rheometer (t_3) is an important intermediary point between extrusion and full cure. Once t_3 is passed, a print should have greater success with overhanging geometry because it is less likely to deform under small forces applied by the nozzle and potentially the silicone weight. The measurement of yield stress values was limited by the safe operational boundaries of the rheometer, and the last yield stress value reported in this work should not be taken as the last yield stress of the elastomer in general. However, these yield stress measurements are appropriate to describe the time period when uncured printed parts are more vulnerable to disruption and failure. When a previous silicone layer reaches the point of fastest cure rate (t_4) it is in one of the best positions to receive a newly deposited layer because there are theoretically still enough uncured areas available for chemical bonding while having a much higher G' at 34 kPa. Determining how many chemical bonds are available from t_4 to full cure would be valuable to coordinate to adhesion properties of the layers, but that study is left to future work. A full cure at t_5 provides the best layer stiffness because the silicone is a solid elastomer. However, adhesion between a cured and uncured layer may not be as strong as the adhesion between two uncured layers. This total cure time is more likely to apply to a region of previously printed layers than to one layer itself due to the 24.9 min until full cure at 30°C.

Making silicone prints of various morphologies confirmed that controlling the rheology and curing kinetics enabled silicone printing without support. It also revealed printing limitations when it came to complex geometries (overhanging structures in multiple directions, layers building on top of nonvertical walls). For this work, models (and therefore layer times) were increased in size until they were stiff enough to maintain structural integrity. A study exploring the geometrical limits of the silicone printer in each curing stage was left to future work. Still, each printed layer should be able to hold a few vertical centimeters of material according to normal force testing (Supplementary Figs. S3 and S4). The geometrical limits of the prints are also determined by the maximum overhang angle. Overhang angle is an interesting limitation because just-mixed silicone has similar values of initial G' regardless of temperature (Supplementary Fig. S2). This means that when the silicone is extruded within the first few minutes, the overhang angle in the newest deposited

layer is largely determined by the silicone formulation and the available support area of the immediate layer below it. However, once the print is layered and curing, the overhang angle of a stack of layers is determined by the cure state of the silicone, as uncured overhangs will collapse under enough deposited weight (Supplementary Fig. S4). The transient cure state of both the individual layers and printed model regions can be estimated to achieve desired print quality. This analysis can also be generally applied to other thermoset materials used in printers with mixing extruders.

Future work

Future work on this printer will include a full parametric study of overhang angle versus wall thickness, as well as aspect ratio limit tests at each cure stage. Currently, the prints are completed within the optimal time frame, but the exact cure state of each printed layer within that transient region is unknown. One aspect of this work that will also be explored further is the strength of adhesion between layers based on deposition time and cure state. In addition, modeling the transient curing between the t_1 and t_5 data points through a predictive equation is planned to correlate percent cure, geometrical limitations, and final mechanical behavior(s). This modeling can hopefully be combined with extruder path planning to further optimize the stability of the model during printing and its final mechanical properties. The effect(s) of the printer design on the printed filament quality, especially at higher temperatures, will also be investigated. The printer build instructions will be distributed as an open-source system, including both the hardware and printing methods. This leaves room for continuous improvement and collaborative development in the soft device community.

Conclusion

In summary, we report a framework for how to 3D print a thermoset silicone without support by using its transient material properties during curing. This framework is built upon rheological and curing kinetics characterization to determine boundaries for time and temperature to predict development of crosslinking in the silicone. Using this method, several models are printed with a custom Dragon Skin 10 Very Fast formulation, which have hollow and overhang geometries. This framework expands upon previous work by facilitating the 3D printing of soft elastomeric structures that do not require support material or a fluid support bath. These methods can be applied to other curing chemistries to further elucidate the role of rheology and curing in transient material systems for additive manufacturing.

Acknowledgments

The authors thank the members of mLab for their continued support and production of prototype 3D models for this work. This work was supported by the Office of Naval Research Young Investigator Program (ONR YIP N00014-16-1-2529; P.O. Tom McKenna).

Author Disclosure Statement

No competing financial interests exist.

Supplementary Material

Supplementary Data
Supplementary Figure S1
Supplementary Figure S2
Supplementary Figure S3
Supplementary Figure S4
Supplementary Figure S5
Supplementary Figure S6
Supplementary Figure S7
Supplementary Figure S8
Supplementary Movie S1

References

1. Hardin JO, Ober TJ, Valentine AD, *et al.* Microfluidic printheads for multimaterial 3D printing of viscoelastic inks. Adv Mater 2015;27:3279–3284.
2. Lipton JI, Angle S, Lipson H. 3D printable wax-silicone actuators. Annu Int Solid Free Fabr Symp 2014;2014: 4–6.
3. Kolesky DB, Truby RL, Gladman AS, *et al.* 3D bioprinting of vascularized, heterogeneous cell-laden tissue constructs. Adv Mater 2014;26:3124–3130.
4. Lind JU, Busbee TA, Valentine AD, *et al.* Instrumented cardiac microphysiological devices via multimaterial three-dimensional printing. Nat Mater 2017;16:303–308.
5. Ober TJ, Foresti D, Lewis JA. Active mixing of complex fluids at the microscale. Proc Natl Acad Sci 2015;112: 12293–12298.
6. Periard D, Malone E, Lipson H. Printing Embedded Circuits. 18th Solid Freeform Fabrication Symposium, Austin, TX, 2007:6–8.
7. Morrow J, Hemleben S, Menguc Y. Directly fabricating soft robotic actuators with an open-source 3-D printer. IEEE Robot Autom Lett 2017;2:277–281.
8. Yirmibesoglu OD, Morrow J, Walker S, *et al.* Direct 3D printing of silicone elastomer soft robots and their performance comparison with molded counterparts. IEEE Int Conf Soft Robot RoboSoft 2018;2018:295–302.
9. Frutiger A, Muth JT, Vogt DM, *et al.* Capacitive soft strain sensors via multicore-shell fiber printing. Adv Mater 2015; 27:2440–2446.
10. Shan S, Kang SH, Raney JR, *et al.* Multistable architected materials for trapping elastic strain energy. Adv Mater 2015; 27:4296–4301.
11. Coulter FB, Ianakiev A. 4D printing inflatable silicone structures. 3D Print Addit Manuf 2015;2:140–144.
12. Yuk H, Zhao X. A new 3D printing strategy by harnessing deformation, instability, and fracture of viscoelastic inks. Adv Mater 2017;1704028.
13. Discov3ry 2.0 Complete. Struct Print Go Plast. Available at: https://www.structur3d.io/discov3ry-2-complete/ Accessed November 17, 2017.
14. ACEO® Silicones - Introducing a new material for 3D printing. ACEO. Available at: https://www.aceo3d.com/silicones/ Accessed November 17, 2017.
15. picsima3d. picsima3d. Available at: www.picsima.com Accessed January 17, 2017.
16. German RepRap GmbH. Available at: https://www.germanreprap.com/myfactory/web/cms/home-en.aspx?WPParams=43CCD7D4B5DDE6B7C2E0B1CDE1C8B6B79495 Accessed April 30, 2018.

17. Our Process. Carbon 3D. Available at: https://www.carbon3d.com/process/ Accessed May 18, 2018.
18. Lipton JI, Cohen D, Heinz M, *et al.* Fab@Home model 2: Towards ubiquitous personal fabrication devices. Solid Free Fabrciation Symp 2009;70–81.
19. Bhattacharjee T, Zehnder SM, Rowe KG, *et al.* Writing in the granular gel medium. Sci Adv 2015;1:e1500655.
20. O'Bryan CS, Bhattacharjee T, Hart S, *et al.* Self-assembled micro-organogels for 3D printing silicone structures. Sci Adv 2017;3:e1602800.
21. Hinton TJ, Hudson A, Pusch K, *et al.* 3D printing PDMS elastomer in a hydrophilic support bath via freeform reversible embedding. ACS Biomater Sci Eng 2016;2:1781–1786.
22. Kokkinis D, Bouville F, Studart AR. 3D printing of materials with tunable failure via bioinspired mechanical gradients. Adv Mater 2018;1705808.
23. Raney JR, Lewis JA. Printing mesoscale architectures. MRS Bull 2015;40:943–950.
24. Truby RL, Lewis JA. Printing soft matter in three dimensions. Nature 2016;540:371–378.

Address correspondence to:
Dr. Stephanie Walker
CoRIS Institute
Oregon State University
204 Rogers Hall
Corvallis, OR 97331

E-mail: walkerstephwork@gmail.com

Dr. Yigit Menguc
Facebook Reality Labs
Redmond, WA 98052

E-mail: yigit.menguc@oculus.com